Journal of Nuclear Materials 403 (2010) 204–215

Contents lists available at ScienceDirect

Journal of Nuclear Materials

journal homepage: www.elsevier.com/locate/jnucmat

Review

Thermodynamic and transport properties of thoria–urania fuel of Advanced Heavy Water Reactor

M. Basu (Ali), R. Mishra, S.R. Bharadwaj, D. Das *

Chemistry Division, Bhabha Atomic Research Centre, Trombay, Mumbai 400 085, India

ARTICLE INFO

Article history:
Received 13 May 2008
Accepted 13 January 2010

ABSTRACT

High temperature thermochemistry of thoria–urania fuel for Advanced Heavy Water Reactor was investigated. Oxygen potential development within the matrix and distribution behaviors of the fission products (fps) in different phases were worked out with the help of thermodynamic and transport properties of the fps as well as fission generated oxygen and the detailed balance of the elements. Some of the necessary data for different properties were generated in this laboratory while others were taken from literatures. Noting the behavior of poor transports of gases and volatile species in the thoria rich fuel (thoria–3 mol% urania), the evaluation shows that the fuel will generally bear higher oxygen potential right from early stage of burnup, and Mo will play vital role to buffer the potential through the formation of its oxygen rich chemical states. The problems related to the poor transport and larger retention of fission gases (Xe) and volatiles (I, Te, Cs) are discussed.

Contents

1. Introduction

India accounting for about one-third of the world's thorium reserve [1] is implementing thoria utilization programme through three-stage fuel cycle concept – viz., plutonium (^{239}Pu) generation from uranium in pressurized heavy water reactors (PHWR), ^{233}U breeding from the naturally abundant ^{232}Th isotope in fast breeder reactors (FBR), and ^{233}U burning for power production using PWR/FB reactors. India is also exploring the possibility of direct utilization of thorium in Advanced Heavy Water Reactor (AHWR) configuration [2].

* Corresponding author. Tel.: +91 22 25595102; fax: +91 22 25505151.
E-mail address: dasd@barc.gov.in (D. Das).

0022-3115/$ - see front matter © 2010 Elsevier B.V. All rights reserved.
doi:10.1016/j.jnucmat.2010.01.009

In AHWR, thoria-based fuels will be used and the fuel will contain 2–4% fissile isotopes of uranium (^{233}U) or plutonium (^{239}Pu) in the mixed oxide forms: $Th_{1-y}U_yO_2$, and $Th_{1-y}Pu_yO_2$. In such a reactor, while the U/Pu isotopes undergo fission by thermal neutrons there is simultaneous burning of the abundant isotope ^{232}Th via in situ generation of the daughter atom ^{233}U. About 60% of the AHWR power output is anticipated to be from the thorium burning process. AHWR being a new concept, its technological [2] implementation needs the input of basic data of physics and chemistry of the fuel and its fission products (fps). The data will help to understand whether the physical and chemical evolution of the fuel during long irradiation period is conducive for safe operation of the reactor.

A burnup of about 50 GWD ton^{-1} will be common in the thoria-based fuel considering its reprocessing difficulty due to the presence of fast decaying ^{232}U isotope ($t_{1/2}$ = 73.6 y) to gamma active daughters (^{212}Bi, 0.7–1.8 MeV, and ^{208}Tl, 2.6 MeV). To attain an average discharge burnup of 50 GWD ton^{-1} with a typical power rating of 18–20 kW m^{-1} in AHWR, the fuel will be irradiated for over 60 months. During the irradiation, the fuel pin (Fig. 1a) generally bears the thermal profile of 1300–1500 K as the central temperature and 800–900 K as peripheral temperature (Fig. 1b), and occasionally above this range in power ramp situation. At the high temperatures and under the steep thermal gradient, the fps undergo transport and redistribution within the cladded pin (Fig. 1a), and chemically react among themselves and with the thoria matrix and clad. Under this situation integrity of fuel pin and clad is the main issue. The integrity is governed by the physicochemical transformation of the fuel matrix and clad with burnup.

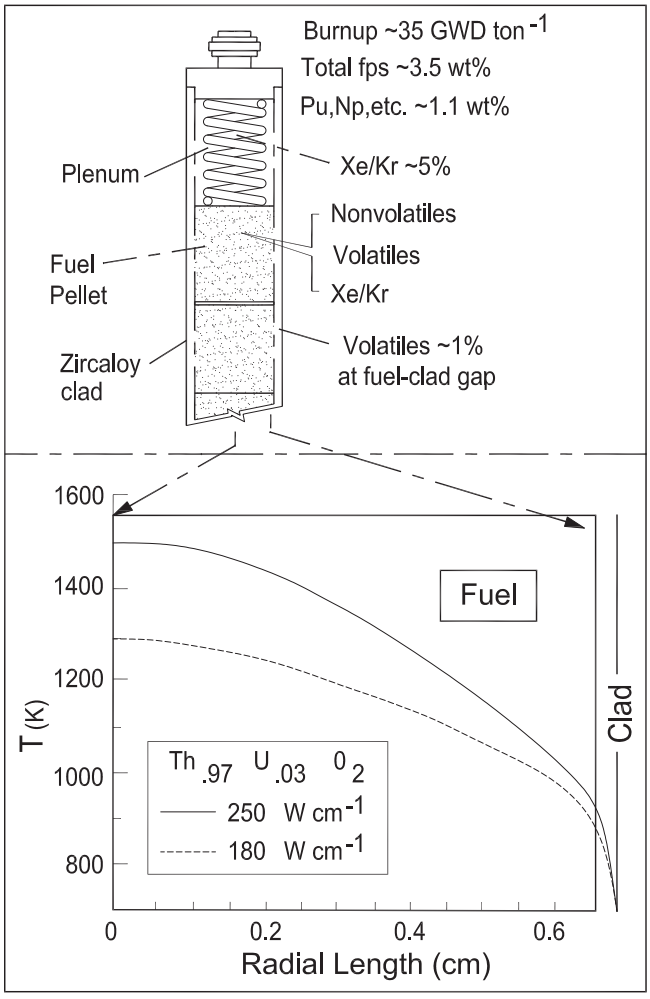

Fig. 1. (a) Schematic of cladded fuel pin (top). (b) Typical thermal profile in the fuel at 35 GWD ton^{-1} (bottom).

For the analysis and evaluation of the fuel–clad integrity during long irradiation period, the knowledge of thermodynamic and transport properties of the fuel and fps is a necessity. Using these information, one evaluates: (i) concentration built up of gaseous and corrosive volatile species at the fuel–clad interface, (ii) the possible extent and path ways of chemical damage of the clad by the corrosive volatiles, and (iii) the extent of fuel swelling and disintegration by the gas accumulation and different solid phase formations inside the fuel matrix.

The above mentioned aspects, though well-known for the conventional urania fuel, need to be re-established for new fuel like thoria. Thoria (ThO_2) has quite a number of advantages over urania (UO_2) like better thermal transport and thermomechanical properties, higher chemical stability and radiation resistance ensuring better in-pile performance and a more stable waste form [3–5]. Like the case of the conventionally used oxide fuels, thoria-based fuels do not pose any difficulty in handling and fabrication, at least in the virgin state. Typically, thoria–3 mol% urania solid solution for AHWR is fabricated by intimately mixing the constituent oxides in a ball-mill and sintering the material in pellet form made under a pressure of 150 MPa. The sintering is carried out in programmed furnace under atmosphere of nitrogen–8% hydrogen at 1923 K over several hours achieving thereby a density greater than 96% TD with average grain size of 55 μm.

2. Distinguishable features of thoria-based fuels and the general scenario of the fission products inside thoria matrix

The fuel chemistry with thoria is not expected to be the same as that experienced with urania in the conventional reactors, though the same set of fps with similar yields (Table 1) are formed and settle down inside the MO_2 fluorite lattices with similar crystal radii of the cations (M = Th^{+4}, U^{+4}). Different chemistry of thoria originates from unique four valency of Th in its compounds as against flexible valency of four to six for U. Urania can be oxidized to hyperstoichiometric composition UO_{2+x}, and by this it can buffer oxygen released during fission to a large extent. Oxygen is released as the actinide metal M in MO_2 matrix (M = Th, U, Pu) undergoes fission. The chemical affinity for oxygen being absent in ThO_2, the buffering action will be evidently weak in thoria-based fuels. For the same reason the oxygen transport in the fuel is predominantly by self diffusion unlike the case in urania where oxygen makes faster transport through the chemical affinity driven diffusion process. These subtle features can lead to faster growth of oxygen pressure in the thoria-based fuels and alter the thermochemistry of fps.

The oxygen released during fission gets redistributed among reactive fps, fuel and clad for their oxidations. The states of oxidized fps inside urania matrix are fairly well established and are summarized in Table 2 for typically high burnt fuel of pressurized water reactor [6]. Like urania, fluorite lattice of thoria can accommodate many of the fps in oxides, metallic and gaseous phases. The alkaline earth thorates $MThO_3$ can be chemical components in the grey (perovskite) phase. Additionally, there can be tetragonal/cubic phases due to alkali thorates of composition M_2ThO_3. Considering, however, the stated subtle features of thoria one needs to address to a number of specific issues such as how fast and to what extent the oxygen pressure inside the thoria-based fuels grows with burnup, whether the O-pressure growth could be buffered by the oxidation of reactive fps and clad, or, whether there could be oxygen transport impediment in thoria rich matrix

Table 1
Integrated values of fission products yields from reactor fuels at their respective burnup.

Fps (atom%)	^{235}U PWR	MOX (7.8%PuO_2) PWR	^{233}U AHWR	^{239}Pu FBR
Burnup (GWD T^{-1})	45	45	20	100
Y + RE	25.3	23.1	26.6	23.4
Ba + Sr	7.2	5.3	9.4	5.3
Zr	13.3	9.5	16.7	9.8
Cs + Rb	11	10.8	9.8	11
Mo	11.7	11	10.3	10.7
Ru + Tc + Rh + Pd	16	23.8	7.1	22.9
Xe + Kr	12.8	12.8	16.2	12.6
Metalloids + halogens	1.8	2.2	2.8	2.4
Ag + Sn + Cd	0.7	1.4	0.3	1.2

Table 2
Chemical states of fps in oxide fuels.

Types of fps	Chemical states
Non-volatiles	
Rare-earths (Nd, La, Ce, etc.) and transition metals (Y, Zr, Nb)	Dissolved state in fuel matrix (MO_2)
Alkaline earths (Sr, Ba) and Zr, U, Pu, Mo, Ce	Perovskite, $M'M''O_3$ (grey) phase
Noble metals (Pd, Ru, Rh, Tc) and Mo	Alloy (white) phases
Gases and volatiles	
Inert gases (Xe, Kr)	Dispersed microbubbles in fuel Fractional release at fuel–clad gap and at plenum
Alkali metals (M = Cs, Rb)	MI, M_2Te at low-moderate burnup Conversion of MI, M_2Te to uranate/molybdate at high burnup
Cd, Te, Sb	In alloy phases
Te, I, Br	As alkali metal compounds

to result in much higher oxygen potential than in urania. If the oxygen potential is high then there are other issues pertaining to increase in free iodine concentration and formation of oxygen rich bulky phases. These later issues become important when Mo oxidation to buffer oxygen potential is slow.

In order to address the stated issues, one makes a detailed balance of oxygen released during fission considering its consumption by the fps, fuel and clad according to their oxidation hierarchies to different chemical states. The detailed balance requires thermodynamic as well as kinetic data of oxidation of the fps, oxygen transport properties inside the matrix and across the fuel–clad gap, and oxygen incorporation kinetics in zircaloy clad.

3. Detailed O-balance from thermodynamic and kinetic analyses

Intercomparison of the reported oxygen potentials of the fps oxides [7] leads to the fact that at first yttrium and rare earths (RE) will be oxidized to their respective trivalent oxides and this will be followed by the oxidation of alkaline earths (Sr, Ba) and zirconium to their divalent and tetravalent oxides respectively. Zr in zircaloy clad will be oxidized approximately at the Zr/ZrO_2 potential. The extent of oxidation of the other fps (Cs, Mo, etc.) less oxidizable than Zr cannot be deduced without considering the thermodynamic stabilities of their ternary compounds. To understand oxygen redistribution among the fps, the O-potentials of the relevant metal/metal oxide systems are plotted as functions of temperature in Fig. 2a while the O-potential of the fuel, $Th_{0.97}U_{0.03}O_2$ at typically two different temperatures is indicated

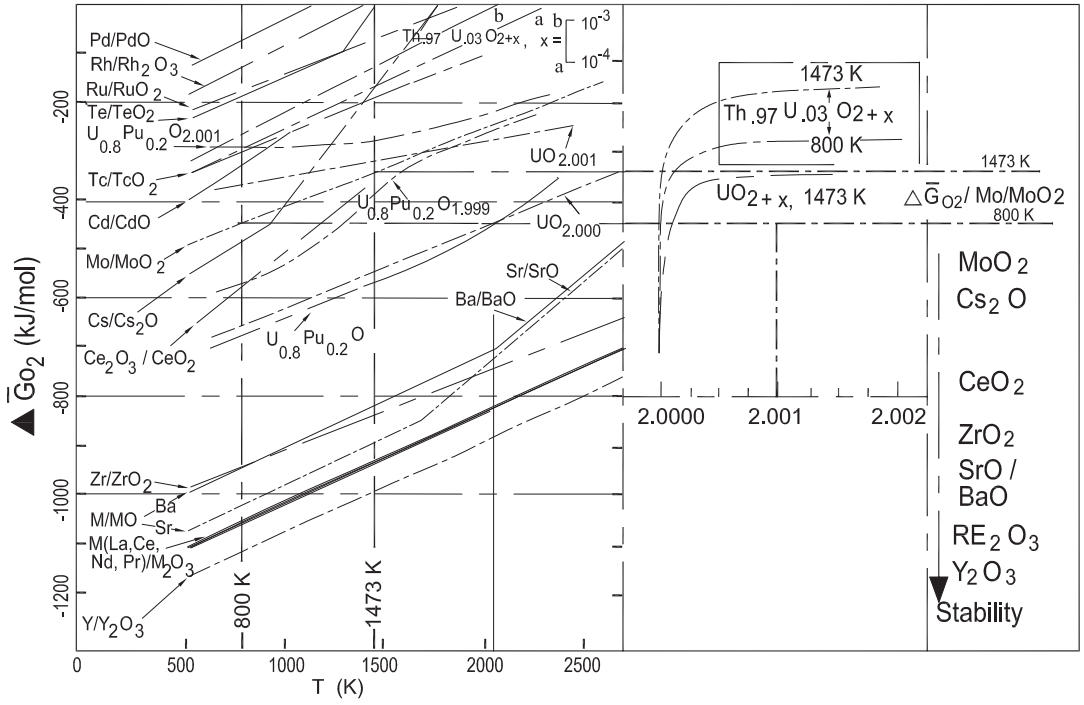

Fig. 2. (a) Oxygen potential of fission product/fp-oxide systems. (b) Oxygen potential of AHWR fuel. (c) Fission products' oxides formation hierarchy.

in Fig. 2b. The hierarchal oxides are indicated in Fig. 2c. Fig. 2b indicates that the O/M ratio in the fuel will hardly rise from the typical initial value of 2.0000 when the O-potential of the fuel attains to that of Mo/MoO_2. In urania fuel, in contrast, the O/M ratio at 1473 K should rise to the value of 2.001 (Fig. 2b) before Mo gets oxidized.

Referring to the fps yields in AHWR fuel (Table 3), the rare earth, alkaline earth, and zirconium can consume about 87.2% of oxygen released during fission in forming their respective binary oxides RE_2O_3, SrO, BaO, CeO_2 and ZrO_2 (Table 3). CeO_2 gets stabilized as cerate components in the perovskite (grey) phase, (Ba,Sr)(Zr,Th, U,Ce)O_3, constituted mainly of the alkaline earth zirconates. From the balance amount of 12.8% oxygen a part would be transported to clad while the rest part of O will be used for the oxidations of Cs/Rb, fuel and Mo. To understand the redistribution behavior of the balanced 12.8% oxygen, a brief mention is now made of the thermodynamic aspect of the alkali fps states and kinetic aspects of the O-transport and oxidation of clad.

3.1. Thermodynamic aspects of alkali fps

Fig. 3 shows the oxygen potentials of relevant chemical equilibria involving Cs. The metal oxide phases have O-potentials roughly 200 kJ mol^{-1} above that of Zr/ZrO_2, and almost the same amount below that of Mo/MoO_2 (not included in the figure). The potential values for the different oxide systems indicated in Fig. 3 were obtained from our experimental results and reported information [8–17] as summarized in Table 4. The formations of O-rich ternary compounds of Cs starts taking place when the remaining 12.8 atom% of fission generated oxygen raises the O-potential above that of Zr/ZrO_2. The extent of O-uptake by Cs/Rb depends on the amounts of O-partitioning among the possible ternaries: thorates/zirconates and uranates/molybdates. The alkali thorate formation would be favored to the zirconates as Zr preferentially forms the more stable alkaline earths zirconates. The kinetics aspect comes into play in the oxygen uptakes as the competing reactants, thoria, urania, and Mo-alloy, have restricted accessibilities for Cs due to its very low diffusion. With the low urania content in AHWR fuel and very small quantity of the evenly dispersed alloy phase, Cs uptake by thoria matrix as $2[Cs] + 1/2O_2(g) + ThO_2(s) = Cs_2ThO_3(s)$ will be kinetically dominating before undergoing conversion into thermodynamically favored states like uranates and molybdates as $Cs_2ThO_3(s) + [UO_2] + 1/2O_2(g) = ThO_2(s) + Cs_2UO_4(s)$ and $Cs_2ThO_3(s) + [Mo]_{alloy} + 3/2O_2(g) = ThO_2(s) + Cs_2MoO_4(s)$. Out of the two, the former reaction is preferred because it calls for a lesser number of oxygen molecules to undergo transport. Under very low oxygen pressure, kinetics of oxygen transport makes the preference. In urania based fuel Cs is known to be fixed in the uranate form [18]. Because of U-233 isotope production in thoria-based fuel the initial urania content of 3 mol% will hardly be lowered [19] and therefore, whatever little Cs is generated can get fixed as uranate. With the AHWR yield of the alkali metals, 10 out of the 12.8 leftover oxygen will be used (one O per Cs atom) in the uranate formation (Table 3).

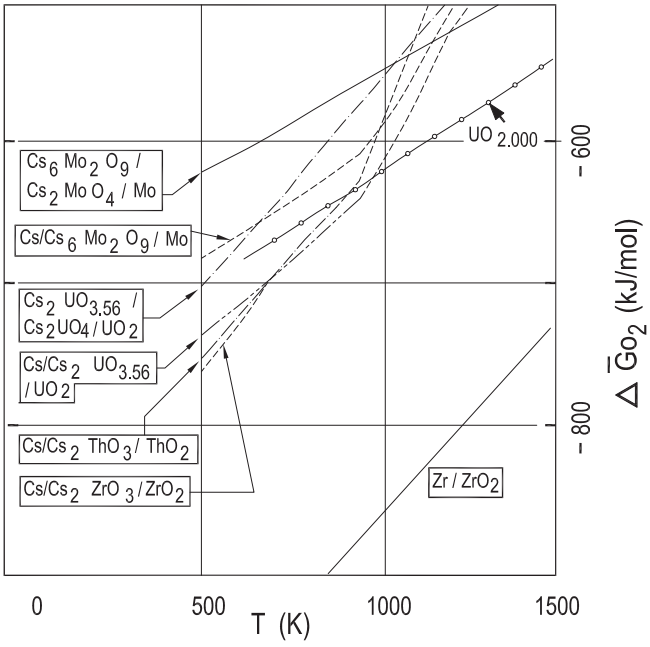

Fig. 3. Relevant chemical states of Cs.

If for kinetic reason all Cs and Rb were remaining as cesium and rubidium thorates, the oxygen balance would have been set to 7.8 atom% instead of 2.8% obtained from the purely thermodynamic considerations. The actual value of oxygen balance will lie somewhere in between. Any augmented consumption of oxygen by the alkaline earth molybdates/uranates formation is not possible, as their formations require BaO/SrO components to be displaced from the more stable perovskite phase. In the absence of detailed information of the cesium transport and alloy phase distribution in the matrix, the kinetic aspect is difficult to quantify. Rest of the presentation is thus based on the redistribution of the residual oxygen of 2.8% obtained from thermodynamic considerations. This

Table 3
Oxygen uptake by the fission products of AHWR fuel.

fps ($^{233}UO_2$ = 2FPs + 2O)	fps% yield in AHWR ThO_2–$^{233}UO_2$ fuel	Oxide type/other possibilities	O-content
Y + RE	27	M_2O_3	40.5
Ba + Sr	9	MO	9
Zr	17	MO_2	34
Ce part in RE	7.4	CeO_2 from Ce_2O_3	3.7
O-uptake by reactive fps			87.2
Cs + Rb	10	M_2O	<5
		M_2UO_4 from $M_2O + UO_2$ (some Cs as CsI, Cs_2Te)	<5
O-uptake by reactive fps + alkali metals			<97.2
Mo	10	>1.4% Mo as MoO_2	>2.8
Pd + Ru + Tc + Rh	8	Alloy phase with Mo	100 (total sum O)
Xe + Kr	16	Gas	
Metalloid + halogen	3 (1.8 + 1.2)	CsX, Cs_2Te	

Table 4
Summary of thermodynamic data of relevant ternary compounds of the fission products.

Ternary compounds (molar volume w.r.t. ThO_2 at ambient)	$\Delta_f G_T^0$ kJ mol^{-1} $800 \leqslant T \leqslant 1500$ K	Ternary compounds (molar volume w.r.t. ThO_2 at ambient)	$\Delta_f G_T^0$ kJ mol^{-1} $800 \leqslant T \leqslant 1500$ K	Ternary compounds (molar volume w.r.t. ThO_2 at ambient)	$\Delta_f G_T^0$ kJ mol^{-1} $800 \leqslant T \leqslant 1500$ K
$BaThO_3$ (orthorhom bic; 1.31)	$-1802 + .279T$ [8]	$BaZrO_3$ (cubic; 1.6)	$-1787 + 0.2954T$ [10]	Cs_2MoO_4 (orthorhombic; 2.28)	$-1514 + 0.3605T$, $T < 952$ K; [10]
				Hexagonal	$-1649.6 + 0.5209T$, $T > 952$ K [10]
				Cs_2MoO_4(liq)	$-1611.3 + 0.4897T$, $T > 1229.5$ K [10]
$SrThO_3$ (monoclinic; 1.47)[a]	$-1825 + 0.29T$ [9]	Cs_2ThO_3 (cubic; 1.57)	$-1780 + 0.44T$ [14]	$SrMoO_4$ (tetragonal; 2.12)	$-1540.6 + 0.3576T$ [10]
$BaUO_3$ (orthorhom bic; 1.32)	$-1687 + 0.2705T$ [10,11]	Rb_2ThO_3 (cubic; 1.65)	$-1822 + .45T$ [15]	$BaMoO_4$ (tetragonal; 2.02)	$-1555.5 + 0.387T$ [17]
$BaMoO_3$ (cubic; 1.41)	$-1229 + 0.2615T$ [10,12]	Cs_2ZrO_3 (orthorhombic; 1.93)	$-1672 + 0.44T$ [16]	$SrUO_4$ (tetragonal; 1.27)	$-1980.2 + 0.34T$ [10]
$SrMoO_3$ (cubic; 1.63)	$-1269 + 0.2702T$ [13]	Cs_2UO_4 (tetragonal; 1.51)	$-1926 + 0.4108T$, $T < 952$ K; $-2062 + 0.5532T$, $T > 952$ K [10]	$BaUO_4$ (orthorhombic; 1.32)	$-1988.8 + 0.3597T$ [10]

[a] Orthorhombic $SrThO_3$; 1.41.

will give a lower limit of oxygen potential rise in fuel or Mo/zircaloy oxidations. The 2.8% of the oxygen released during fission is constantly available from 0.0125 m dia. fuel pellet at 18 kW m^{-1} power rating will result in the O-flux of 5.2×10^{-11} g atom s^{-1} m^{-1} and O-flux density (B) of 4.6×10^{-7} g atom m^{-3} s^{-1}.

3.2. Kinetic aspects of residual flux of fission-released oxygen

The kinetic path of O-transport at a steady flux of 5.2×10^{-11} g atom O s^{-1} m^{-1} to clad will be governed by the slowest one of the three processes in series: (a) transport through matrix, (b) transport across fuel–clad gap, and (c) oxidative incorporation in clad, which are briefly described below. Parallely, the fission product Mo present in metallic precipitate can consume the residual part of oxygen forming MoO_2 component. The relative consumptions of oxygen in the two parallel paths depend on their relative kinetics.

3.2.1. Transport through matrix

Oxygen transport by self diffusion $D_{ox}(T)$ in pure thoria and urania matrices are quite comparable [20,21] as respectively given by $D_{ox}(m^2\ s^{-1}) = 4.5 \times 10^{-4}\exp(-275\ kJ\ mol^{-1}/RT)$ and $D_{ox}(m^2\ s^{-1}) = 2.6 \times 10^{-5}\exp(-251\ kJ\ mol^{-1}/RT)$. For urania, studies show that the self diffusion contribution is several orders of magnitude lower than chemical diffusion $D_{ox,\ c}\ (T)$ contribution, which is given by [22] $D_{ox\ c}(m^2\ s^{-1}) = 1.8 \times 10^{-6}\exp(-90\ kJ\ mol^{-1}/RT)$. For thoria-based matrix there is very little information on the chemical diffusion property of oxygen. Matsui et al. [23] have reported the oxygen chemical diffusion property in $Th_{1-y}U_yO_{2+x}$ ($y = 0.2$ and 0.4) with activation energies quite similar in magnitude to that of pure urania. Their data reflect non-linear decrease of the transport coefficient with lowering of the urania content in the ternary solution as shown in Fig. 4. The oxygen transport study of SIMFUEL (20 GWD ton^{-1} burnup) with very low urania content ($Th_{0.98}U_{0.02}O_{2+x}$) as carried out in this laboratory conforms to the non-linear decline in the transport indeed (Fig. 4). Such non-linear drop in diffusivity is expected from the behavior of oxygen potential of the fuel formulated by thermochemical approach [24]. The experimental data at the limit of $x = 0$ can be represented as $D_{ox\ c}(\pm 0.25\ m^2\ s^{-1}) = 1.5 \times 10^{-9}\exp(-103\ kJ\ mol^{-1}/RT)$. The orders of magnitude difference in diffusion coefficients shows that thoria-based fuels with low urania content will have significant impediment in the oxygen transport as compared to the urania case. The oxygen profile evolution in the two fuel matrices can be made considering the redistribution of the 2.8% of the left over oxygen in the respective cases.

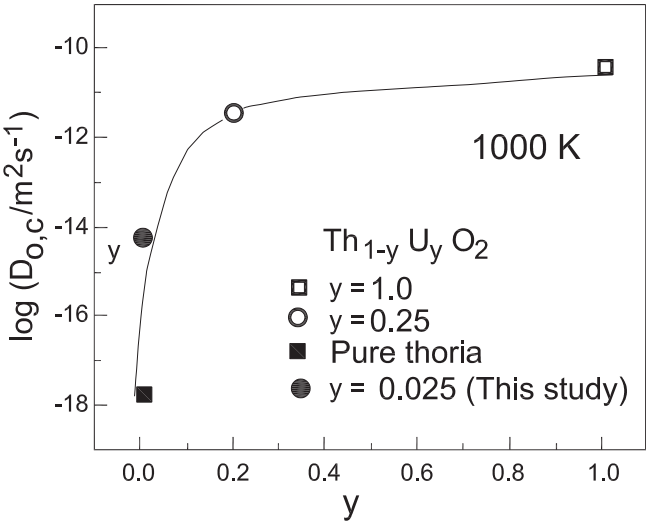

Fig. 4. Trend of oxygen transport coefficient with urania content in $Th_{1-y}U_yO_{2+x}$ at $x = 0$.

3.2.2. Oxygen transport across fuel–clad gap

The steady flux of 2.8% of oxygen released during fission to be radially transported to clad by gaseous diffusion across the helium filled annular gap of about 50 μm needs a pressure drop of 10^{-10} bar or more for O. This will be feasible with the oxygenated species such as $H_2O(g)$, $Cs_2O(g)$ and $CsOH(g)$ [25] since by the available hydrogen gas and cesium vapor their partial pressures on the fuel surface will be much above 10^{-10} bar according to the equilibrium reactions: $MO_{2+x} + \delta H_2(g) = MO_{2+x-\delta} + \delta H_2O(g)$, $MO_{2+x} + 2\delta Cs(g) = MO_{2+x-\delta} + \delta Cs_2O(g)$, etc. Sources of hydrogen are moisture impurity in the fuel, nuclear reaction (n,p), diffusion influx from zircaloy-coolant reaction (by nuclear reaction itself, around 1.8×10^{-4} hydrogen isotopes are produced per 100 atoms of fps at a burnup of 20 GWD ton^{-1}). Reported growth kinetics of oxide layer (S) in zircaloy [6] are high enough to take care of the residual O-flux from the fuel.

With the reported value of fuel expansion of 0.6% per 10 GWD ton^{-1} burnup a fuel pin of diameter 12 mm will expand to fill up the gap of 50 μm by the time it reaches 30 GWD ton^{-1}. After this the direct transport of oxygen to zircaloy becomes operative and it is more efficient as compared to vapor phase transport.

4. Oxygen profile evaluation

It is important to know the steady state oxygen profile under which the constant O-flux of 5.2×10^{-11} g atom s^{-1} m^{-1} can be transported out to the fuel boundary, where its concentration is fixed by low oxygen potential of the clad. On the approximation of radial diffusion of species under chemical and thermal potential gradients in the pellet, the steady state oxygen flux $J(r)$ across the cylindrical section of radius r and unit height is given by $J(r) \equiv \pi r^2 B = 2\pi r C_O\,[-D_{O,c}\partial \ln x_O/\partial r - D_O(Q/RT^2)(\partial T/\partial r)]$. B is volume density of the O-flux (4.6×10^{-7} g atom m^{-3} s^{-1}), C_O is the interstitial oxygen concentration (C_O/x_O being the total oxygen concentration in MO_{2+x}). D_{ox} and $D_{ox,\,c}$ self and chemical diffusion coefficients respectively for $Th_{1-y}U_yO_{2+x}$, and R is the gas constant. The first term within the square bracket is contributed by entropy rise in transferring one gram atom of oxygen under the concentration gradient. For the mass transfer, the oxide lattice transports electrically charged oxygen vacancy or interstitial in the opposite direction and thus performs the minimum thermoelectric work of $\delta W = -\bar{S}_O\,dT$ which is positive under negative $\partial T/\partial r$. The work under the thermal gradient manifests out of a minimum heat expense of $|T(\delta W/dT)| \equiv \bar{S}_O T$ from the lattice. The overall minimum heat expense of $\bar{S}_O T$ contributing to the second term of $J(r)$ expression in fact debits a portion of the entropy rise expressed through the first term. The negative value of $Q(\leqslant -\bar{S}_O T)$ has been reported by several investigators [26] from the measured oxygen redistribution in hyper- and hypo-stoichiometric urania–plutonia fuel under steady state. In the absence of such data for $Th_{0.98}U_{0.02}O_2$ based SIMFUEL, the O-profile was evaluated considering the magnitude of Q/T as $\bar{S}_O$, which according to the reported O-potential behavior of $Th_{0.98}U_{.02}O_{2+x}$ is 12 J K^{-1} g $atom^{-1}$ [24]. For $D_{ox,\,c}$ values the stated SIMFUEL result, namely, $D_{ox\ \ c}(\pm 0.25\ m^2\ s^{-1}) = 1.5 \times 10^{-9}\exp(-103\ kJ\ mol^{-1}/RT)$ was used. For D_{ox}, the molar mean value of reported self diffusion coefficients of ThO_2 and UO_2 [20,21] in $Th_{0.98}U_{0.02}O_2$ was used as $D_{ox}(m^2\ s^{-1}) = 4.2 \times 10^{-4}\exp(-275\ kJ\ mol^{-1}/RT)$.

The evaluated O-profile in the SIMFUEL of the cylindrical matrix of diameter 0.0125 m is given in Fig. 5. The steady state of temperature profile in the fuel is included in the figure. The evaluated radial concentration of interstitial oxygen, x in MO_{2+x}, is seen to vary from 0.004 to 0.001. Similar evaluation for urania fuel under identical temperature gradient and steady O-flux showed orders of magnitude lower concentration, which is mainly due to very high O-diffusion in urania. The temporal evolution of oxygen concentration can be expressed [27] considering a simpler situation with an average diffusivity over the thermal profile in the cylindrical geometry (diameter $2a = 0.0125$ m). The time constants for attaining steady profile is more than a year for thoria as against an hour or so for urania.

The constantly available flux due to 2.8% of the fission-released oxygen to be transported out of the fuel, the oxygen potential profile should stand orders of magnitude above that of Mo/MoO_2 (Fig. 5). If the flux is fully used in Mo oxidation then the potential profile will be that of Mo/MoO_2. The result of such calculation thus shows the important role of Mo for buffering the oxygen potential in the thoria-based fuel. Considering reported oxidation rate of Mo surface [28] together with the fact that freshly generated Mo can undergo faster oxidation one concludes that Mo can easily buffer the oxygen potential.

5. Transport properties of fission gases and volatile fission products

For integrity analysis of fuel, the knowledge of release characteristics of gaseous and volatile fps is important. The release significantly deteriorates the gap conductance while the retention

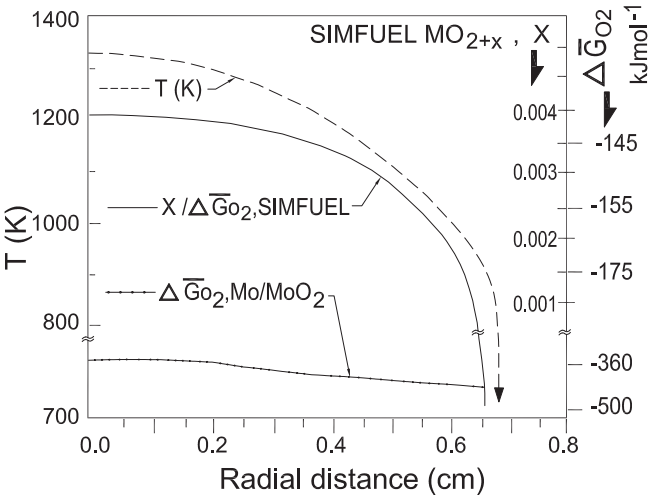

Fig. 5. Steady state radial-oxygen-profile in thoria–2 mol% urania SIMFUEL at 20 GWD ton^{-1} under O-flux of 5.2×10^{-11} g atom s^{-1} m^{-1} of fuel rod (thermal profile, and Mo/MoO_2 potential profiles are also included).

generates stress inside matrix. The gases having negligible solubility in the fuel matrix, retained fraction gets dispersed as microbubbles and results in fuel swelling.

During the last decades extensive studies have been made on transport behavior of gases and volatiles in urania and urania–plutonia fuels. Similar studies on the thoria-based fuels are only a few [29] in comparison. Studies generally indicate the subtle difference in their transport properties in urania and thoria matrices. In the former case the diffusion is significantly influenced by O/M ratio; the oxygen hyper-stoichiometry augments the diffusion. Th remaining strictly tetravalent in its oxide, the electronegative species such as I and Te is expected to show distinction in their diffusion behaviors as compared to those in urania. The reported value of anion interstitial migration energy (Q_i) is significantly higher in thoria (3.27 eV) than in urania (2.6 eV) while the vacancy migration energy (Q_v) is comparable (~0.8–1.0 eV) [20,30]. The gaseous and volatile species are expected to diffuse using interstitial and vacancy sites in the lattice. Reported experimental data for O-diffusion show that the activation barrier for the diffusion is higher in thoria (2.8 eV) [21] than in urania (2.6 eV) [20].

5.1. Fission gas transport properties

Matzke et al. [31,32] found little or no effect of dopants such as Nb_2O_5, Y_2O_3, and La_2O_3 on the diffusion property of Xe implanted in urania and thoria matrices. The study further indicated that Xe atom does not diffuse through cation or anion vacancies but through the trivacancies out of one metal and two O sites (Schottky trios). Theoretical calculation also ascribed to the trivacancy mechanism for Xe diffusion [33]. Naik et al. [34] and Kaimal et al. [35] studied Xe diffusion in trace irradiated specimens of urania and thoria–1 mol% urania in pellets and powdered forms with and without the dopants Nb_2O_5, Y_2O_3. Their results showed two to five times drop in Xe diffusivity in the doped samples. Cation or anion vacancy not augmenting the transport, these authors made similar conclusion as that of Matzke et al. In a recent study in this laboratory it has been shown that increase of both cation and anion vacancies augments Xe transport substantially [36]. The vacancies were introduced in the simulated fuel (ThO_2–2 mol% UO_2 containing fission products corroborating to 20 GWD ton^{-1} burnup) by evaporation of magnesia component in thoria and also of SrO/BaO components from the added alkaline earth fps in the SIMFUEL

during its long sintering at 1900 K in flowing argon containing 8% hydrogen.

With the increase of irradiation dose, the Xe diffusivity at any temperature is found to fall progressively and beyond a dose of 10^{23} fission m^{-3} the diffusivity levels off to orders of magnitude lower values [29,32,37]. The lowering has been interpreted to be due to formation of radiation induced defects (damages) that act as nucleation centers for the supersaturated gas atoms to accumulate as 'trapped'[38,39] micro bubbles leading to heterogeneity in the diffusion path. Shiba et al. [37,40] noted that the Xe release is dependent on urania concentration in thoria ($0 \leqslant X_{UO2} \leqslant 20$ mol%) and it attains minimum at 5–6 mol% urania content. Reported capsule irradiation of $(Th,U)O_2$ pellet samples at high burnup [41] however indicated no bearing of the U/Th ratio on the fission gas release.

The typical temperature dependence of D_{Xe} at low and high doses reported by different authors [29,32,33] are included in Table 5. Thermal annealing of radiation induced defects makes slight deviation in the activation energy at higher temperature. The barrier energy of 478 kJ mol^{-1} obtained by Shiba et al. [40] can be compared with those reported for urania by different authors: 407 kJ mol^{-1} by Miekeley and Felix [42], 376 kJ mol^{-1} by Matzke [20] and 644 kJ mol^{-1} by Prussin et al. [43] Shiba et al. explained the observed barrier energy by invoking that Xe transport occurred through tetra vacancy mechanism [44]. Trivacancy introduction through evaporation of alkaline earth oxides in the SIMFUEL resulted in reduction in barrier energy as well as increase in frequency factor for Xe diffusion [36] (Table 5).

5.2. Volatile products transport properties

Early studies [45–47] have indicated that iodine diffuses in thoria-based matrix at a comparable rate as that of Xe. Naik et al. [48], however, showed contrasting behavior in I and Xe diffusion. By studying I transport in ThO_2–0.1%UO_2 pellet samples of bulk densities of 79–90% theoretical value, it is shown that I undergoes transport using the anionic sublattice; the deduced activation energy (248 kJ mol^{-1}) [Table 6] is comparable to that of anion self diffusion in thoria (~270 kJ mol^{-1}). Further, by increasing the irradiation dose from 5.5×10^{20} to 1.1×10^{23} fission m^{-3}, they found two fold rise in I transport coefficient unlike Xe. At high dose, I can make faster resolution from gas bubbles due to its affinity for anionic vacancy sites and make augmented transport using radiation induced defects/damages in the lattice. Transport study of ion implanted Xe and Rb, Cs, Te, I, and Br also show similar contrast between the inert gas and the volatiles. Matzke et al. and Verrall et al. [49–52] in fact showed that the volatiles segregate as microbubble/precipitate when their ions are implanted at high dose (~$1.5–2 \times 10^{20}$ ions m^{-2}).

Transport and release behaviors of I and Te in trace irradiated (~5×10^{20} fission m^{-3}) thoria–2 mol% urania with and without doping of fps were studied in this laboratory [53,36]. Isothermal release kinetics of I as well as Te was very low as compared to the reported results of ion implanted studies, and contrasting features were noted in the virgin and SIMFUEL matrices with nearly identical grain characteristics (37–45 μm size, 9500 kg m^{-3} density, 25 m^2 kg^{-1} BET surface). Fig. 6 shows the typical cumulative release of ^{131}I and ^{132}Te from the fuel specimens as function of annealing time at 1773 K. After initial burst release, the cumulative value of iodine attained steady parabolic growth. Contrastingly, for virgin fuel [53], the growth gradually deviated from the steady value to practical halt. The halting in I release is interpreted to be due to electric field built up inside the lattice through preferential transport of anionic I as compared to the cationic counterpart Cs (or, Rb) that diffuses sluggishly unless the temperature is too high [54]. For tellurium, the steady growth of released fraction was attained soon after the burst release in both the fuel matrices. The transport parameters of I and Te deduced from parabolic growth of their cumulative releases are included in Table 6. For comparison, the reported behaviors in pure urania fuel matrix [43,55] are also included. In virgin fuels both the volatile species are shown to have slower transports in thoria than in urania. In simulated fuel lattice the anionic vacancies were introduced mainly by the dissolution of the trivalent rare earths and effect of this is reflected in the lowering of barrier energy for both I and Te. Unlike iodine tellurium's high tendency of mixing in metallic components is reflected in its larger drop in the frequency factor in SIMFUEL as compared to the virgin case.

The transport and release behaviors of the alkali metal fission products reported for ion implanted thoria, urania and their SIMFUEL matrices [56,52,57] showed that at low dose, Rb and Cs behave in a similar way to Xe. The release from thoria is slow as compared that from urania. The release patterns from thoria and its SIMFUEL are nearly the same. The early study [57] reports the transport parameters D_0 and Q as $10^{-4\pm1}$ m^2 s^{-1} and 418 ± 19 kJ mol^{-1} respectively. At high implantation dose (~$1.5–2 \times 10^{20}$ ions m^{-2}) the Cs/Rb release show no retardation due to trapping phenomenon evidenced in the case of Xe.

The isochronal study with Cs in irradiated thoria–6% urania by Akabori et al. [54] showed that Cs release is extremely low as compared the reported high release from the ion implanted sample.

Table 5
Transport properties of Xe in oxide fuel.

Authors	System studied	Diffusivity, $D = D_0\mathrm{Exp}[-Q/RT]$
Matzke [20]	Xe/urania, trace irradiation	$D_0 = 5.0 \times 10^{-5}$ m^2 s^{-1} $Q = 376$ kJ mol^{-1}
Naik [29]	Xe/urania, 5×10^{20} fission m^{-3}	$D_0 = 4.9 \times 10^{-11}$ m^2 s^{-1} $Q = 272$ kJ mol^{-1}
Naik [29]	Xe/thoria–1% urania, 5.5×10^{21} fission m^{-3}	$D_0 = 1.4 \times 10^{-12}$ m^2 s^{-1} $Q = 239$ kJ mol^{-1}
Naik [29]	Xe/thoria–1% urania, 1.5×10^{24} fission m^{-3}, $T < 1500$ K	$D_0 = 4.5 \times 10^{-15}$ m^2 s^{-1} $Q = 239$ kJ mol^{-1}
Naik [29]	Xe/thoria–1% urania, 1.5×10^{24} fission m^{-3}, $T > 1500$ K	$D_0 = 5.3 \times 10^{-13}$ m^2 s^{-1} $Q = 289$ kJ mol^{-1}
Shiba [39]	Xe/thoria–6% urania, 0.9×10^{21} fission m^{-3}	$D_0 = 2.6 \times 10^{-5}$ m^2 s^{-1} $Q = 478$ kJ mol^{-1}
Shiba [39]	Xe/thoria–6% urania, 1×10^{23} fission m^{-3}	$D_0 = 7.1 \times 10^{-11}$ m^2 s^{-1} $Q = 344$ kJ mol^{-1}
Present study [36]	Xe/thoria–2% urania SIMFUEL (20 GWD T^{-1}) with created trivacancies, 5.5×10^{20} fission m^{-3}	$D_0 = 1.5 \times 10^{-10}$ m^2 s^{-1} $Q = 189$ kJ mol^{-1}

Table 6
Transport properties of I, Te and Cs in oxide fuel.

Authors	System studied	Diffusivity, $D = D_0\mathrm{Exp}[-Q/RT]$
Dharwadkar [55]	I/urania, 5×10^{20} fission m^{-3}	$D_0 = 5.3 \times 10^{-10}$ m^2 s^{-1} $Q = 294$ kJ mol^{-1}
Prussin [43]	I/urania	$D_0 = 2.7 \times 10^{-2}$ m^2 s^{-1} $Q = 510 \pm 138$ kJ mol^{-1}
Prussin [43]	Te/urania	$D_0 = 6.9 \times 10^{-3}$ m^2 s^{-1} $Q = 481 \pm 46$ kJ mol^{-1}
Naik [48]	I/thoria–0.1% urania, 5×10^{20} fission m^{-3}	$D_0 = 1.3 \times 10^{-7}$ m^2 s^{-1} $Q = 248$ kJ mol^{-1}
Kaimal [53]	I/thoria–2% urania, 5×10^{20} fission m^{-3}	$D_0 = 1 \times 10^{-11}$ m^2 s^{-1} $Q = 286$ kJ mol^{-1}
Kaimal [53]	Te/thoria–2% urania, 5×10^{20} fission m^{-3},	$D_0 = 2.1 \times 10^{-4}$ m^2 s^{-1} $Q = 491$ kJ mol^{-1}
Present study [36]	I, Te/thoria–2% urania SIMFUEL (20 GWD T^{-1}) with created trivacancies, 5.5×10^{20} fission m^{-3}	$D_0 = 1.4 \times 10^{-14}$ m^2 s^{-1} $Q = 162$ kJ mol^{-1}, for I $D_0 = 3.9 \times 10^{-12}$ m^2 s^{-1} $Q = 260$ kJ mol^{-1}, for Te
Akabori [54]	Cs/thoria–6% urania, 1×10^{24} fission m^{-3}	$D_0 = 1.16 \times 10^{-6}$ m^2 s^{-1} $Q = 463$ kJ mol^{-1}
Akabori [54]	Cs/thoria–6% urania, 1×10^{25} fission m^{-3}	$D_0 = 4.46 \times 10^{-1}$ m^2 s^{-1} $Q = 664$ kJ mol^{-1}

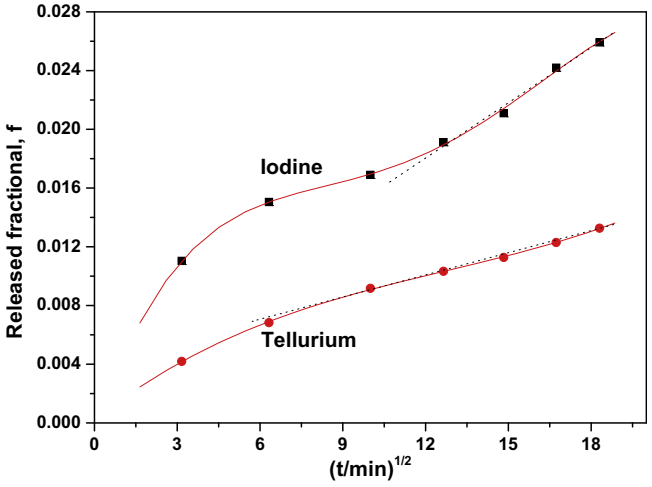

Fig. 6. Typical release plot of I and Te from Simfuel at 1773 K.

The transport parameter D_0 for Cs obtained using moderately irradiated samples (1×10^{24} fission m^{-3}) is about two orders of magnitude lower than the reported value from ion implantation experiments. The activation energy of 463 kJ mol^{-1} is quite in agreement with ion implantation result. At higher irradiation dose (3×10^{25} fission m^{-3}), the Cs release sharply falls and the derived activation energy rises by 200 kJ mol^{-1} [54].

6. Evaluation of high burnup fuel chemistry in thoria-based matrix

Thermodynamic and kinetic data show that a certain percentage of oxygen released during fission could neither be consumed by more reactive fps, nor be transported out to clad in thoria rich fuel. Mo has the vital role in consumption of the left over oxygen after the formation of binary oxides of yttrium and rare earths, alkaline earths and zirconium, and ternary oxides (molybdates and uranates) of alkali fps. For assessment of the chemical states of the oxidized molybdenum one considers the effect of thermodynamic activities of Mo and other components participating in the

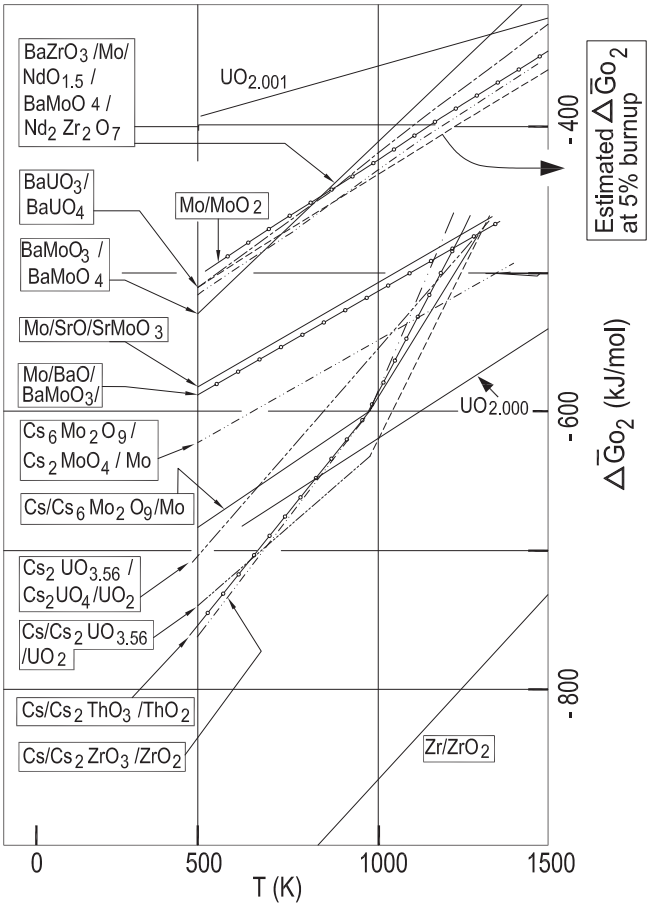

Fig. 7. Oxygen potentials of relevant oxide systems at different temperatures.

oxidation equilibria. The comparative representation for the potential (Fig. 7) of pseudo-binary, ternary, and other equilibria involving pure phases of the fps indicates that in the proximity of Mo oxidation several oxygen-rich phase components have their formation possibilities: (a) $[Mo]_{alloy} + O_2(g) + [AO] = [AMoO_3]$, (b)

$2[Mo]_{alloy} + 3O_2(g) + 2[AO] = 2[AMoO_4]$, and (c) $2[AZrO_3] + [R_2O_3] + 2[Mo] + 3O_2(g) = [R_2Zr_2O_7] + 2[AMoO_4]$, where $AMoO_3$ and $AMoO_4$ (A = Ba/Sr) represent perovskite and scheelite-type phase components respectively, and $R_2Zr_2O_7$ is the pyrochlore of the rare earths (R = La, Nd, etc.).

To evaluate the oxygen potential that decides the order of participation of the different oxidative equilibria, one finds out at first the Mo and MoO_2 activities in the equilibrium as $[Mo] + O_2 = [MoO_2]$. The values of a_{Mo} depend on Mo content in alloy phase, which generally varies from 20% to 40% [58] depending on the fuel composition, irradiation pattern and burnup. For the thoria-based fuel, considering the low solubility of MoO_2 in thoria (<0.2 mol%) and the extent of alkali molybdate formation, Mo remains mostly in alloy phase. At 50 GWD ton^{-1} burnup, the Mo content works out to be about 34%. Taking note of the experimental results of Yamawaki et al. [59], the hexagonal alloy phase with 34% Mo content can have a_{Mo} values of 0.25–0.3 within the fuel temperatures of 800–1500 K. In the present analysis, a value of 0.3 for a_{Mo} is used all through. The a_{MoO2} values, on the other hand, can be estimated from the stipulation that 2.8% of the oxygen released during fission is oxidizing Mo to form either $BaMoO_3$/$SrMoO_3$ perovskite components or MoO_2 phase itself. High values of BaO and SrO activities would facilitate the molybdite states. Again relative activities of the two oxides decide the MoO_2 partitioning according to the equilibrium, $[BaMoO_3] + [SrO] = [BaO] + [SrMoO_3]$, that has marginal change in the standard free energy as, $\Delta G^0_{reaction} = -3.2 + 0.008T$ kJ mol^{-1}. As BaO attains higher stability in zirconate perovskite than SrO, the MoO_2 partitioning will preferably be as $SrMoO_3$.

For $SrMoO_3$ formation each Mo atom consuming 2 oxygen, the 2.8% remains of oxygen released during fission will lead to 0.028 mol of the molybdite per fission. This is so as one fission yields two oxygen from the oxide fuel. If all of Ba yield (Y_{Ba} = 0.064 per fission) in AHWR is fixed as $BaZrO_3$ while the 2.8% remain of oxygen is fixed as $SrMoO_3$, then the ratio of molybdite is to zirconate is 0.028/0.064. When X_{BaZrO3} value is greater than 0.5, the X_{SrMoO3} will be above 0.22. The molybdite solubility in the Ba-rich zirconate phase would decide whether such a high concentration can be accommodated in the perovskite. As there is no reported data of $SrMoO_3$ solubility in the zirconate, one refers to the reported solubility of the $BaMoO_3$ (X^s = 0.46 at T = 1973 K) in $BaZrO_3$ [60]. The regular solution parameter ($\alpha \sim 41.3$ kJ mol^{-1}) obtainable from the solubility data provides means of extrapolation of X^s to lower temperatures using $d\ln X^s/d(1/T) = -H^{excess}/R$, $H^{excess} = \alpha(1 - X^s)^2$. X^s becomes 0.36 at 1473 K. The solubility of $SrMoO_3$ in Ba-rich zirconate phase is assumed to be around the same value (36 mol%) at 1473 K. The ratio of $SrMoO_3$ to $BaZrO_3$ being at 0.028/0.064 (~0.44), the molybdite will remain dissolved in the perovskite.

6.1. SrO activity estimation

From consideration of higher stabilities of zirconates than cerates, the reported presence of Ce in the perovskite phase (Ba,Sr)(Zr,Ce)O_3 [61] is neglected to a first approximation while making the estimation for SrO and BaO activities. It is further assumed from the stability point of view that ZrO_2 partitioning as $SrZrO_3$ is less than as $BaZrO_3$. The SrO activity can be obtained considering the upper and lower limits respectively obtainable from two criteria: (i) the reaction $[ZrO_2] + [SrO] = [SrZrO_3]$ under the stipulation of $a_{SrZrO3} < 0.5$ in its equilibrium property, $RT\ln(a_{SrO}) = \Delta G^0_{reaction} + RT\ln(a_{SrZrO3}/a_{ZrO2})$, ($\Delta G^0_{reaction}$ being the standard free energy change of the reaction) and (ii) the reported absence of the pyrochlore, $Nd_2Zr_2O_7$ [61] as product of the reaction $2[SrZrO_3] + 2[NdO_{1.5}] = Nd_2Zr_2O_7(s) + 2[SrO]$ so that $RT\ln a_{SrO} > [-\Delta G^0_{reaction} + RT\ln(a^2_{SrZrO3}\, a^2_{NdO1.5})]/2$. Required $NdO_{1.5}$ activity is approximated to the idealized value of completely dissolved state of this oxide component ($X_{NdO1.5} \sim 0.042$) in the thoria-based SIMFUEL of 21.5 atom% burnup. ZrO_2 activity required in (i) is obtained considering the concentration of dissolved part of ZrO_2 in thoria at burnup B and the solution property of zirconia in thoria. Until saturation ZrO_2 concentration in the fuel at burnup β (fissile atom%) is approximately expressed as $X_{ZrO2} \approx (Y_{Zr} - Y_{Ba})\beta/100$, Y_{Zr} (~0.33) and Y_{Ba} (~0.064) being the average yields of Zr and Ba per fission; $X_{ZrO2} \sim 0.0027\beta$. The reported evaluation of ZrO_2 solubility in thoria [62] to be represented as $\ln X^0_{ZrO2} = 1.67 - 7510/T$, provides the value of the regular solution parameter (45.2 kJ mol^{-1}), which can be used to estimate the oxide activity as $RT\ln(a_{ZrO2}/X_{ZrO2}) = 45.2(1 - X_{ZrO2})^2$.

Iteratively, the obtained span of a_{SrO} limits can be narrowed down towards the lower limit with a converged value of a_{SrZrO3} as 0.25. The perovskite phase if approximated as the mixture of $BaZrO_3$, $SrZrO_3$ and $SrMoO_3$, their idealized concentrations with the value of X_{SrMoO3}/X_{BaZrO3} as 0.44 works out to be $X_{BaZrO3} = 0.52$, $X_{SrZrO3} = 0.25$ and $X_{SrMoO3} = 0.23$. The median of a_{SrO} limits turns out to be $RT\ln a_{SrO} = -115.7 + (0.047 - 0.0083\ln\beta)T$. The dissolved part of ZrO_2 in the fuel calculated earlier on the basis of $BaZrO_3$ partitioning only will be somewhat modified due to $SrZrO_3$. For example, with the ZrO_2 partitioning as 25 mol% $SrZrO_3$ and 75 mol% $BaZrO_3$, the X_{ZrO2} would reduce to 0.0024β from the previously accounted 0.0027β.

6.2. BaO activity estimation

To get MoO_2 and ZrO_2 partitioning respectively into the molybdites and zirconates of the two alkaline earths, the knowledge of BaO activity is also required as elaborated below.

BaO being common to all the perovskite components, $BaMO_3$ (M = Zr, Ce, U, Th), its activity can be assessed from the equilibria, $[MO_2] + [BaO] = [BaMO_3]$, where MO_2 is a dissolved component in fuel phase. Like the SrO case, the BaO activity evolves with the burnup and is essentially governed by the equilibrium behavior of the most stable perovskite component $BaZrO_3$. Thus in the equilibrium reaction $[ZrO_2] + [BaO] = [BaZrO_3]$, one considers $BaZrO_3$ as the predominant component in the perovskite phase with a concentration greater than 50 mol% and lesser than 75 mol%. It is to be noted that these limits fall well within the perovskite composition used thus far: $X_{SrZrO3}/X_{BaZrO3} = 0.33$, and $X_{SrMoO3}/X_{BaZrO3} = 0.44$; i.e., $X_{SrZrO3} = 0.187$, $X_{SrMoO3} = 0.248$ and $X_{BaZrO3} = 0.565$. Accordingly, the lower and upper limits of the BaO potential were expressed as $-174 + (0.048 - 0.0083\ln\beta)T$ kJ mol^{-1} > $RT\ln a_{BaO} > -174 + (0.045 - 0.0083\ln\beta)T$ kJ mol^{-1}. The median of the two limits is $-174 + (0.0465 - 0.0083\ln\beta)T$ kJ mol^{-1}.

The limiting values of BaO activity can also be obtained by making use of the reported EPMA results of the SIMFUEL, that is, $Th_{0.933}U_{0.067}O_2$ fuel matrix that is doped with the rare earths, Y, Zr, Sr, Ba, Mo, Ru, and Rh for 21.5% FIMA [61] and annealed at 1873 K under an oxygen potential (−309.6 kJ mol^{-1}) below that of Mo/MoO_2 [63]. The result indicates that the Th, U, and Mo contents in the perovskite phase remained below the EPMA resolution of about 1 atom%. Thoria and urania in the SIMFUEL behaving ideally their activities would remain at 0.933 and 0.067 respectively. Therefore, their equilibria with perovskite components $BaThO_3$ and $BaUO_3$ as $[BaO] + [AcO_2] = [BaAcO_3]$, (Ac = Th, U) together with the consideration. of the EPMA resolution limits for $BaAcO_3$ components, the BaO activity is obtainable from the relation, $RT\ln(a_{BaO}) = \Delta G^0_{reaction} + RT\ln(a_{BaAcO3}/a_{AcO2})$. In $BaUO_3$ case, one can approximate $BaUO_3$ activity to its concentration from the observed complete miscibility of $BaUO_3$ in $BaZrO_3$ with Vegard's law applicability to lattice parameters [60] in the dilute region of the uranite ($BaUO_3 \leqslant 20$ mol%). The limit, $a_{BaUO3} < 0.01$, results in an upper bound of BaO activity in the fuel at 1873 K. One can make

similar assumption for $BaThO_3$ component also. The estimated BaO activities at 1873 K was extrapolated to lower temperatures using the arrived temperature trend of a_{BaO} in $[ZrO_2] + [BaO] = [BaZrO_3]$. Yet another limiting value of BaO activity can be obtained from $BaCeO_3 - CeO_2$ equilibrium by considering an upper bound of the cerate concentration in the perovskite as 10 mol% [58] and CeO_2 concentration in thoria as per the fission yield of Ce. CeO_2 is completely miscible in thoria [64,65]. $BaCeO_3$ activity and regular solution parameter (-40.16 kJ mol^{-1}) obtainable from the reported tensimetric data (640–780 K) of $BaZrO_3$–$BaCeO_3$ solution [66] leads to the high temperature activity values.

Other limiting values of BaO activity can be derived from the observations [61] that Mo is absent in the perovskite phase and pyrochlore phase $(La,Nd)_2(Zr,Ce)_2O_7$ is not formed out of the reaction, $Nd_2O_3 + 2[BaZrO_3] = Nd_2Zr_2O_7 + 2[BaO]$. $BaMoO_3$ to be formed out of $[Mo] + O_2(g) + [BaO] = [BaMoO_3]$ remaining below the EPMA resolution, gives an upper limit of a_{BaO}. The pyrochlores absence gives a lower limit of a_{BaO}. The BaO potential ($RT \ln a_{BaO}$) obtained out of the different thermochemical routes is represented in Fig. 8. The upper limits obtained from the different consideration were seen to fall over a large stretch of the potential values. In view of their large uncertainties, the two limits obtained out of the equilibrium $[ZrO_2] + [BaO] = [BaZrO_3]$ (lower shaded region in Fig. 8) were considered for expressing the median potential (the dotted line in Fig. 8) given by $RT \ln a_{BaO} = -174 + (0.0465 - 0.0083 \ln \beta)T$ kJ mol^{-1}.

Considering the estimated activities of SrO and BaO, the standard free energy change of MoO_2 partitioning in the reaction $[BaMoO_3] + [SrO] = [BaO] + [SrMoO_3]$ can be expressed as $RT \ln(a_{BaMoO3}/a_{SrMoO3}) = -61.5 - 0.007T$ kJ mol^{-1}. The result is indicative of MoO_2 partitioning predominantly as $SrMoO_3$ and it is essentially due to significantly low BaO potential out of large stability of $BaZrO_3$. Similarly, for ZrO_2 partitioning in the reaction $[SrZrO_3] + [BaO] = [SrO] + [BaZrO_3]$ one writes $RT \ln(a_{SrZrO3}/a_{BaZrO3}) = -0.2 - 0.0075T$ kJ mol^{-1} and this indicates that $SrZrO_3$ activity is lower than that of $BaZrO_3$ (e.g., $a_{SrZrO3}/a_{BaZrO3} = 0.4$ at 1000 K).

6.3. Oxygen potential estimate

The Mo oxidation in the thoria rich fuel is expected to begin from the initial burnup stage. For such situation the oxygen potential can be estimated by considering the equilibrium $[Mo] + O_2(g) + [SrO] = [SrMoO_3]$. Recalling the arrived expression of SrO potential and activities of Mo in alloy phase and $SrMoO_3$ in perovskite as 0.3 and 0.248, one obtains the oxygen potential as $\Delta\bar{G}_{O2} = -559.4 + (0.105 + 0.0083 \ln \beta)T$ kJ mol^{-1}. The oxygen potential could be expressed with ±20 kJ/mol span due to the two a_{SrO} limits. The burnup dependence arises from SrO potential decrease due to ZrO_2 activity augmentation with burnup and at 5 atom% burnup, $\Delta\bar{G}_{O2}$ can be expressed as $\Delta\bar{G}_{O2} = -559 + 0.12T$ kJ mol^{-1}. As seen in Fig. 7, this potential is marginally lower than that of Mo/MoO_2 in the working temperature region of the fuel.

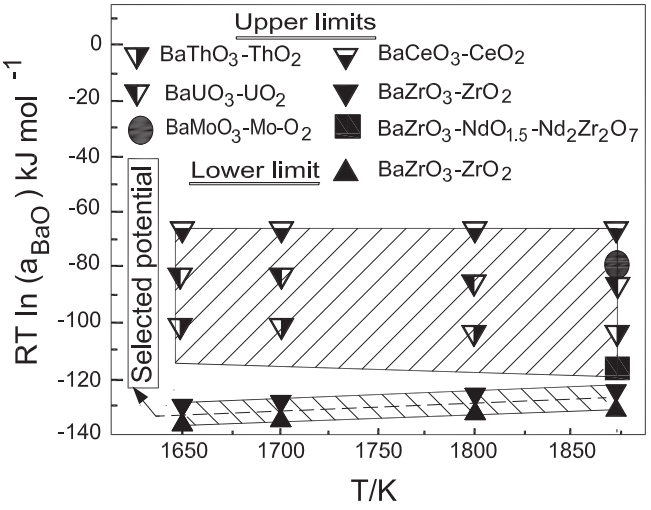

Fig. 8. Evaluated activity limits of BaO in high burnup thoria-based fuel.

One can examine with the oxygen potential whether oxygen-rich compounds (Fig. 7) such as Sr/Ba-molybdates can have significance in the oxygen buffering. Free energy considerations of the reaction, $2[SrMoO_3] + O_2 = 2SrMoO_4(s)$ shows that Sr-molybdite oxidation is not feasible at 5 atom% burnup. Disproportionation of the molybdite forming the molybdate and Mo as $3[SrMoO_3] + [ZrO_2] = [Mo] + 2SrMoO_4(s) + [SrZrO_3]$ also cannot occur. One can examine whether there can be BaO partitioning from zirconate phase to result in pyrochlore and molybdates formation as $2[BaZrO_3] + 2[NdO_{1.5}] + 2[Mo] + 3O_2(g) = Nd_2Zr_2O_7(s) + 2BaMoO_4(s)$. Considering that $NdO_{1.5}$ concentration is $X_{NdO1.5} \sim 0.0016\beta$ and $NdO_{1.5}$ component in thoria behaves ideally, the feasibility of the forward reaction can be evaluated from the inequality $\Delta G^0_{reaction} - RT \ln(X_{NdO1.5} a_{Mo} a_{BaZrO3})^2 - 3\Delta\bar{G}_{O2} < 0$. $\Delta G^0_{reaction}$ was obtained by using the reported data of the pyrochlore [67,68], $Nd_2O_3(s)$ and of the other constituents [63] and was given by $-1808.2 + 0.5516T$ kJ. Taking, for example, the values of a_{BaZrO3} and a_{Mo} as 0.565 and 0.3 respectively, the feasibility of pyrochlore formation can be written as $T < 130/(0.3732 - 0.0415 \ln \beta)$. It shows that even at a burnup like 10%, the forward reaction is absent within the fuel. Under the prevailing oxygen potential, one further shows that the UO_2 oxidation, such as $2[UO_2] + O_2(g) + 2[SrO] = 2SrUO_4(s)$, leading to the formation of alkaline earth uranates is not feasible due to the low activities of the alkaline earth oxides as well as urania in the fuel.

Table 7
Thermodynamic data of oxygen-rich compounds of the fission products.

System	Method/thermodynamic property
$CdMoO_4$	Solution calorimetry, $\Delta_f H°(298.15\ K) = -1034.3 \pm 5.7$(kJ mol^{-1}) [69] Knudsen effusion, $\Delta_f G° = -1002 + 0.267T$ (kJ mol^{-1}) (987 < T < 1033), $\Delta_f G° = -1101.9 + 0.363T$ (kJ mol^{-1}) (1044 < T < 1111) [70]
$ThMo_2O_8$	Solution calorimetry, $\Delta_f H°(298.15\ K) = -2742.2 \pm 4.5$ (kJ mol^{-1}) [71] Transpiration, $\Delta_f G° = -2682.6 + 0.595T$ (kJ mol^{-1}) (1195 < T < 1292) [72]
$UMoO_6$	Transpiration, $\Delta_f G° = -1962.0 + 0.463T$ (kJ mol^{-1}) (1100 < T < 1250) [73]
$La_2Te_3O_9$	Solution calorimetry, $\Delta_f H°(298.15\ K) = -2814.6 \pm 12.9$ (kJ mol^{-1}) [74]
Solution	$La_2Te_4O_{11}$ calorimetry, $\Delta_f H°(298.15\ K) = -3116.5 \pm 17.3$ (kJ mol^{-1}) [74]
Ni_3TeO_6	Transpiration, $\Delta_f G° = -1307 + 0.64T$ (kJ mol^{-1}) (1122 < T < 1202) [75]
$UTeO_5$	Solution calorimetry, $\Delta_f H°(298.15\ K) = -1606.3 \pm 3.5$ (kJ mol^{-1}) [76] Transpiration, $\Delta_f G°(UTeO_5) = -1614.2 + 0.45T$, (kJ mol^{-1}) (1107 < T < 1217) [77] Knudsen effusion, $\Delta_f G°(UTeO_5) = -1616 + 0.40T$, (kJ mol^{-1}) (1063 < T < 1155) [78]
UTe_3O_9	Solution calorimetry, $\Delta_f H°(298.15\ K) = -2287.2 \pm 9.5$(kJ mol^{-1}) [78] Transpiration, $\Delta_f G°(UTe_3O_9) = -2313.1 + 0.89T$ (kJ mol^{-1}) (947–1011)K [77] Knudsen effusion, $\Delta_f G°(UTe_3O_9) = -2318 + 0.80T$, (kJ mol^{-1}) (888–948)K [78]

Table 8
Fractional contribution to fuel swelling by fission product phases.

Fission products	Fp's partitioning into phases	Average molecular volume of the chemical components (Å)^3	Fractional contribution to swelling $Y_i \frac{\Omega_i}{\Omega_{Th}}$
Y, RE, Zr	In fuel phase	40.2	0.73
Mo and noble metals	Alloy phase	14.7	0.11
Ba, Sr	Perovskite phase (Ba, Sr)(Zr, Mo)O3	70.0	0.30
Cs, Rb	(Cs, Rb)2UO4	139.7	0.33

Uranate formation via reduction of SrO component in the fuel phase as $[UO_2] + 2[SrO] = Sr(g) + SrUO_4(s)$ depends on Sr atom transport from the reaction site. The reduction can also result in only gaseous products as $[SrO] + [MO_2] = Sr(g) + MO_3(g)$, (M = U, Mo). The standard free energy changes of the redox reactions ($\Delta G^0_{reaction}$) are 948.2–0.297T kJ mol^{-1} for U and 1006.9–0.295T kJ mol^{-1} for Mo cases respectively. The reacting oxides being present in $SrMoO_3$, its perovskite structure facilitates this reaction kinetically. Under the prevailing oxygen potential and Mo activity, the equilibrium pressures p_{MoO3} and p_{Sr} can be obtainable from $RT \ln p_{MoO3} = -468.3 + 0.10T + 0.0125T \ln \beta)$ kJ mol^{-1}, and $RT \ln(p_{Sr}) = -948.251 + 0.2973T + RT \ln(a_{SrMoO3}/p_{MoO3})$ kJ mol^{-1}. At 1500 K and 5% burnup, p_{Sr} is about 7.7×10^{-8} bar for $a_{SrMoO3} = 0.25$ and it suggests that there will be $SrMoO_3$ volatilization from the central part of the fuel and the transport of the vapor products will ultimately lead to the formation of $SrMO_4(s)$ phase in peripheral part of the fuel pin.

The Mo oxidation keeping pace with the net oxygen release out of the fission in thoria-based fuel, the oxygen-rich phase formation will be largely limited to the molybdite, and to molybdate and uranate in cooler region. For kinetic reason if the oxygen potential surpasses the molybdenum/molybdite-control would lead to the extensive formation of oxide phases like molybdates, tellurites, and tellurates of the fps and clad materials. Summary of the available thermodynamic properties of the oxygen-rich phases [69–78] is included in Table 7. In the conventional oxide fuels, these phases are relevant only for the analysis of failed pin. Oxygen-rich phases as well as the retained gas lead to fuel swelling the extent of which is discussed below.

7. Fuel swelling at high burnup

The thoria-based fuels will develop internal stress from the formation of the bulky oxygen-rich phase and from the large retention of the gaseous products that mostly exist as dispersed gas bubbles. As discussed before, the extent of the fuel swelling from the dissolved and undissolved components of the fps will be more in thoria. The swelling from the undissolved oxygen-rich phases, A_2BO_4 (A = Cs/Rb, B = Mo/U) and $A'BO_4$ (A′ = Ba/Sr) can be worked out as follows:

The contribution to swelling by a solid fission product '*i*' in a particular phase can be expressed considering the burnup (β), molar volume of the oxide fuel (Ω_{Th}) and fission product phase (Ω_i), and yield of the fission product (Y_i). The overall swelling of the fuel with initial number of Th atoms as N^0_{Th} is thus written as [79]:

$$\frac{\Omega_{Th}N^0_{Th}(1-\beta) + \sum \Omega_i Y_i \beta N^0_{Th} - \Omega_{Th}N^0_{Th}}{\Omega_{Th}N^0_{Th}} = \left(\sum Y_i \frac{\Omega_i}{\Omega_{Th}} - 1\right)\beta \equiv \left(\frac{\Delta V}{V}\right)_{\text{solid FPs}}$$

For zirconium the distribution into the fuel phase was worked out taking into account its total yield and its consumption in the perovskite phase formed out of the alkaline fission products. Yttrium and rare earths were considered to be dissolved in the fuel phase. The molybdenum content in the alloy phase was corrected for its partitioning into the perovskite phase. Considering the fission product yield and distribution in different phases the swelling contributions are tabulated (Table 8) at a burnup of 5 atom%. Overall swelling due to the solid fission product phases works out to be 2.3% at this burnup. One expects similar value of the swelling due to solid fission products in urania fuel which is reported to have an overall swelling of (3–3.5)% at 5 atom% burnup in PWR [6]. The difference of (0.7–1.2)% is mainly the swelling contribution from gaseous fission products. The significance of surface energy in gas bubble formation is discussed explicitly in [6] where it is shown that for a given amount of gas dispersed in bubble form the extent of swelling depends on the surface energy and the radius of the bubble. Once the bubble formation starts it occurs in cascade where the role of surface energy is quite insignificant. However, the role of surface energy is significant in deciding the critical radius for nucleation. Since thoria has larger surface energy [80] as compared to urania [81] the gas bubbles will start nucleating with larger radii in case of thoria. The swelling given by [3] $(nRT/2\gamma)r$, suggests that the relative values of (r/γ) for thoria and urania will be the deciding factor to judge the extent of swelling in the respective cases. Therefore uniquely one cannot say that high will promote larger extent of swelling.

8. Conclusions

Thoria-based fuels though have the merit of less thermal dilation, excellent thermal transport properties, good mechanical strength, chemical inertness, and less thermal release of the gaseous and volatile fps, there are certain demerits also. Thoria-based fuel is shown to have poor buffering ability and transport property for oxygen. These make subtle difference in the redistribution of the oxygen released during fission among the fps and clad. Mo oxidation kinetics is shown to play decisive role on the potential buffering all through the burning process. Considering this, the present analysis suggests that the fuel will generally bear higher oxygen potential right from the early stage of burnup. In contrast, the oxygen potential is quite controlled in urania as fission generated oxygen can either oxidize the fuel or undergo faster transport to clad for its oxidation. Mo oxidation in urania occurs at much later stage when the fuel attains high O/M ratio and is morphologically degenerated with dispersed gas bubbles that slow down the transport property. The higher potential in the thoria fuel results in formation of oxidized products like $SrMoO_3$. In the cooler part of the fuel pin, there is likelihood of the formation of more oxidized products like $SrMO_4$ (M = Mo, U). The transport properties of the volatile reactive fps like I, Te, Cs are significantly low in thoria-based fuels as compared to those in urania. The fuel containment problem from the clad corrosion though less in the fuel, the matrix swelling will be more due to the larger retention of gaseous fps and formation of oxygen-rich phases.

References

[1] An overview of world thorium resources, incentives for further exploration and forecast for thorium requirements in the near future IAEA-TECDOC-412 Vienna, 1985, p. 7.
[2] R.K. Sinha, A. Kakodkar, Nucl. Eng. Des. 236 (2006) 683–700.

[3] Annual Report BARC/1999/I/007, pp. 11, 13, 27.
[4] Thorium Fuel Cycle—Potential Benefits and Challenges IAEA-TECDOC-1450 Vienna, 2005, p. 8.
[5] R.P. Agarwala (Ed.), Diffusion Processes in Nuclear Materials, North Holland, 1992. pp. 28, 76.
[6] H. Bailly, D. Menessier, C. Prunier (Eds.), The Nuclear Fuel of Pressurized Water Reactors and Fast Reactors-design and Behavior, Intercept Ltd., 1999.
[7] H. Kleykamp, J. Nucl. Mater. 131 (1985) 221–246.
[8] R. Mishra, M. Ali (Basu), S.R. Bharadwaj, A.S. Kerkar, D. Das, S.R. Dharwadkar, J. Alloys Comp. 290 (1999) 97–102.
[9] M. Ali (Basu), R. Mishra, S.R. Bharadwaj, A.S. Kerkar, S.R. Dharawadkar, D. Das, J. Nucl. Mater. 299 (2001) 165–169.
[10] E.H.P. Cordfunke, R.J.M. Konings, Thermochemical Data for Reactor Materials and Fission Products, Elsevier, Amsterdam, 1990.
[11] T. Matsuda, S. Yamanaka, K. Kurosaki, U. Masayoshi, S. Kobayashi, J. Alloys Comp. 322 (2001) 77–81.
[12] R. Agarwal, Z. Singh, V. Venugopal, J. Alloys Comp. 282 (1999) 231–235.
[13] D.D. Wagman, V.B. Parker, W.H. Evans, I. Halow, S.M. Bailey, R.H. Shuman, K.L. Churney, Selected Values of Chemical Thermodynamic Properties, Nat. Bur. Standard (US), Technical Note 270-6, 1971.
[14] M. Ali (Basu), R. Mishra, A.S. Kerkar, S.R. Bharadwaj, D. Das, S.R. Dharwadkar, J. Nucl. Mater. 282 (2000) 261–263.
[15] M. Ali (Basu), A.N. Shirsat, S.C. Kumar, S.R. Bharadwaj, D. Das, J. Nucl. Mater. 323 (2003) 68–71.
[16] M. Ali (Basu), R. Mishra, S.R. Bharadwaj, A.S. Kerkar, K.N.G. Kaimal, D. Das, J. Alloys Comp. 314 (2001) 96–99.
[17] N.K. Shukla, R. Prasad, D.D. Sood, J. Chem. Thermodyn. 25 (1993) 429–434.
[18] D. Cubicciotti, J.E. Sanecki, J. Nucl. Mater. 78 (1978) 96–111.
[19] Annual Report BARC/1999/I/007, p. 5.
[20] Hj. Matzke, in: R.P. Agarwala (Ed.), Diffusion Processes in Nuclear Materials, North Holland, 1992.
[21] H.S. Edwards, A.F. Rosenberg, J.T. Bittel, ASD-TDR-63-635, 1963.
[22] A.S. Bayoglu, R. Lorenzelli, Solid State Ionics 12 (1984) 53.
[23] T. Matsui, K. Naito, J. Nucl. Mater. 135 (1985) 149–154.
[24] R.P.C. Schram, J. Nucl. Mater. 344 (2005) 223–229.
[25] Proceedings of an International Symposium on Thermodynamics of Nuclear Materials, vol. 1, IAEA, Juelich, Germany, 1979.
[26] C. Sari, G. Schumacher, J. Nucl. Mater. 61 (1976) 192–202.
[27] H.S. Carslaw, J.C. Jaeger, Conduction of Heat in Solids, second ed., Oxford Clarendron Press, 1960.
[28] E.A. Gulbransen, K.F. Andrew, F.A. Brassart, J. Electrochem. Soc. 110 (1963) 952–959.
[29] M.C. Naik, in: R.P. Agarwala (Ed.), Diffusion Processes in Nuclear Materials, North Holland, 1992.
[30] E.A. Colbourn, W.C. Mackrodt, J. Nucl. Mater. 118 (1983) 50.
[31] Hj. Matzke, J. Nucl. Mater. 21 (1967) 190.
[32] Hj. Matzke, Nucl. Applic. 2 (1966) 131.
[33] R.A. Jackson, C.R.A. Catlow, J. Nucl. Mater. 127 (1985) 167.
[34] M.C. Naik, K.N.G. Kaimal, M.D. Karkhanavala, J. Nucl. Mater. 67 (1977) 239.
[35] K.N.G. Kaimal, M.C. Naik, A.R. Paul, Mater. Process. 1 (4) (1990) 293.
[36] A.N. Shirsat, M. Ali (Basu), S. Kolay, A. Datta, D. Das, J. Nucl. Mater. (2008) (under revision).
[37] K. Shiba, A. Itoh, M. Akabori, J. Nucl. Mater. 126 (1984) 18.
[38] J.R. MacEwan, P.O. Morel, Nucl. Appl. 2 (1966) 142.
[39] M.C. Naik, A.R. Paul, K.N.G. Kaimal, Radiat. Eff. 25 (1975) 73.
[40] K. Shiba, in: R.P. Agarwala (Ed.), Diffusion Processes in Nuclear Materials, North Holland, 1992. p. 71.
[41] I. Goldberg, G.L. Spahr, J.F. Giovengo, L.A. Waldman, Trans Am. Nucl. Soc. 27 (1977) 308.
[42] W. Miekeley, F. Felix, J. Nucl. Mater. 42 (1972) 297.
[43] S.G. Prussin, D.R. Olander, W.K. Lau, L. Hansson, J. Nucl. Mater. 154 (1988) 25.
[44] R.W. Grimes, AEA-InTec-0195, 1990.
[45] R.M. Carroll, C.D. Baumann, ORNL-3050, 1961.
[46] Hj. Matzke, R. Lindner, Z. fuer Naturforsch. 159 (1960) 647.
[47] G.W. Parker, G.E. Creek, W.J. Martin, IAEA Panel on Siting of Reactors, Vienna, 1961.
[48] M.C. Naik, A.R. Paul, K.N.G. Kaimal, J. Nucl. Mater. 96 (1981) 57.
[49] R.A. Verrall, Hj. Matzke, T. Ogawa, B.J.F. Palmer, Canada Report AECL-9475, 1986, p. 558.
[50] Hj. Matzke, I.L.F. Ray, R.A. Verrall, Proc. Int. Working Group on Water Reactor Fuel Performance and Technology (Report IAEA, IWGFPT/27, Vienna, 1987, p. 183).
[51] Hj. Matzke, C. Ronchi, Eur. Appl. Rep. 5 (1984) 1105.
[52] Hj. Matzke, R.A. Verrall, J. Nucl. Mater. 182 (1991) 261–264.
[53] K.N.G. Kaimal, A.S. Kerkar, A.N. Shirsat, D. Das, A. Datta, A.G.C. Nair, S.B. Manohar, J. Nucl. Mater. 317 (2003) 189.
[54] M. Akabori, K. Fukuda, J. Nucl. Mater. 186 (1991) 47.
[55] S.R. Dharwadkar, G. Chattopadhyay, S.N. Tripathi, S.R. Bharadwaj, M.C. Naik, A.R. Paul, K.N.G. Kaimal, M.S. Chandrasekharaiah, K.S. Venkateswarlu, IWGFPT/25, IAEA, Vienna, 1986, p. 43.
[56] R.C. Feber, Los Alamos Sci. Lab. Report, LA-Nureg-6635, 1977.
[57] Hj. Matzke, J. Nucl. Mater. 23 (1967) 209.
[58] H. Kleykamp, J.O.A. Paschoal, R. Pejsa, F. Theummler, J. Nucl. Mater. 130 (1985) 426.
[59] M. Yamawaki, Y. Nagai, T. Kogai, M. Kanno, Thermodyn. Nucl. Mater. 1 (IAEA, Vienna, 1980) 249.
[60] J.O.A. Paschoal, H. Kleykamp, F. Thümmler, J. Nucl. Mater. 151 (1987) 10–21.
[61] M. Ugajin, T. Shiratori, K. Shiba, J. Nucl. Mater. 84 (1979) 26–38.
[62] H. Kinoshita, M. Uno, S. Yamanaka, J. Alloy Comp. 370 (2004) 25–30.
[63] I. Barin, Thermochemical Data of Pure Substance, third ed., VCH, Weinheim, 1995.
[64] F. Sibieudeet, M. Foex, J. Nucl. Mater. 56 (1975) 229–238.
[65] O. Kellar, U. Berndt, H. Engerer, L. Leitner, J. Solid State Chem. 4 (1972) 453.
[66] K.H. Ryu, S.M. Haile, Solid State Ionics 125 (1999) 355–367.
[67] S. Lutique, P. Jaborsky, R.J.M. Koenings, J.C. Krupa, A.C.G. van Genderen, J.C. van Miltenburg, M. Wastin, J. Chem. Thermodyn. 35 (2003) 955–965.
[68] D. Sedmiduvsky, O. Benes, R.J.M. Koenings, J. Chem. Thermodyn. 37 (2005) 1098–1103.
[69] M. Ali, S.R. Bharadwaj, D. Das, J. Nucl. Mater. 336 (2005) 110–112.
[70] R. Mishra, S.R. Bharadwaj, D. Das, J. Therm. Anal. Cal. 86 (2006) 547–552.
[71] M. Ali, S.R. Bharadwaj, R. Mishra, A.S. Kerkar, D. Das, Thermochim. Acta 346 (2000) 29–32.
[72] M. Basu, R. Mishra, S.R. Bharadwaj, A.S. Kerkar, S.R. Dharawadkar, J. Nucl. Mater. 257 (1998) 185–188.
[73] S.N. Tripathi, G. Chattopadhyay, A.S. Kerkar, J. Am. Ceram. Soc. 68 (1985) 232.
[74] M. Ali, S.R. Bharadwaj, S.C. Kumar, D. Das, J. Nucl. Mater. 347 (2005) 69–72.
[75] M. Ali (Basu), R. Mishra, A.S. Kerkar, S.R. Bharadwaj, D. Das, J. Nucl. Mater. 301 (2002) 183–186.
[76] M. Basu, R. Mishra, S.R. Bharadwaj, P.N. Namboodiri, S.N. Tripathi, A.S. Kerkar, S.R. Dharwadkar, J. Chem. Thermodyn. 31 (1999) 1259–1263.
[77] R. Mishra, P.N. Namboodiri, S.N. Tripathi, S.R. Bharadwaj, S.R. Dharawadkar, J. Nucl. Mater. 256 (1998) 139–144.
[78] A. Krishnan, G.A. Ramarao, K.D. Singh Mudher, V. Venugopal, J. Nucl. Mater. 254 (1998) 49–54.
[79] B.D. Wirth, D.R. Olander, Nuclear Eng. Dept, Univ. of California, Berkeley, NE120, November 2005.
[80] T. Inoue, Hj. Matzke, J. Am. Ceram. Soc. 64 (1981) 355–360.
[81] R.O.A. Hall, N.J. Mortimer, D.A. Mortimer, J. Nucl. Mater. 148 (1987) 273.